A Parametric Study of the Structure of Hall Magnetic Field Based on Kinetic Simulations. II. Asymmetric Magnetic Reconnection with a Guide Field

Longlong Sang[1,2], Quanming Lu[1,2] , Rongsheng Wang[1,2], Kai Huang[1,2], and Shui Wang[1,2]

[1] CAS Key Lab of Geospace Environment, School of Earth and Space Sciences, University of Science and Technology of China, Hefei 230026, People's Republic of China; qmlu@ustc.edu.cn, rswan@ustc.edu.cn

[2] CAS Center for Excellence in Comparative Planetology, People's Republic of China

Abstract

In this paper, with a two-dimensional (2D) particle-in-cell simulation model, we investigate the structure of Hall magnetic field generated in asymmetric magnetic reconnection with a guide field. It is found that the structure of the Hall magnetic field on the left side of the X line is different from that on the right side. In general, the Hall magnetic field on the left side has a tripolar structure, while it has a bipolar structure on the right side. On the left side of the X line, the Hall magnetic field at the upper and lower parts of the current sheet is positive, while that in the central part is negative. With the increasing guide field, the amplitude of the Hall magnetic field at the upper and center parts of the current sheet decreases, and that at the lower part increases. An increasing asymmetry (either an increase of the ratio of the magnetic field or decrease of the density ratio between the two sides of the current sheet, and the ratio is defined as the values between the side with the stronger magnetic field to that with the weaker magnetic field) leads to the decrease of the Hall magnetic field at the upper part of the current sheet and even disappearance when the asymmetry is sufficiently large, and the increase of the Hall magnetic field at the lower and central parts of the current sheet. On the right hand of the X line, the Hall magnetic field at the upper part of the current sheet is negative, while that at the central part is positive. With the increasing guide field, the Hall magnetic field at the upper current sheet increases, while that at the central current sheet decreases. The increasing asymmetry leads to the decrease of the Hall magnetic field at the upper and central parts of the current sheet, and when the asymmetry is sufficiently large there appears the Hall magnetic field below that at the central current sheet.

Key words: magnetic reconnection – Sun: heliosphere

1. Introduction

Through magnetic reconnection, the stored magnetic energy is released into plasma kinetic energy in a current sheet (Parker 1957; Sweet 1958; Isobe et al. 2005; Drake et al. 2006; Lu et al. 2013; Yamada et al. 2014) and such a process is considered to be responsible for the multiscale natural phenomena from solar flares (Forbes & Acton 1996; Tsuneta 1996; Somov & Kosugi 1997; Birn et al. 2009), coronal mass ejections (CMEs; Gosling & Birn 1995; Lin & Forbes 2000; Roald et al. 2000; Qiu et al. 2004) to substorms in the magnetosphere (Sonnerup 1971; Angelopoulos et al. 2008; Lu et al. 2016; Wang et al. 2016, 2017; Zhou et al. 2017). The mean free path between particles in astrophysical and space plasmas is usually very large, and the collision effect in magnetic reconnection can be neglected (Biskamp & Schwarz 1995; Øieroset et al. 2001; Fu et al. 2006; Huang et al. 2015). During collisionless magnetic reconnection, the decoupled motions between heavy ions and light electrons in the diffusion region lead to the generation of in-plane current, which produces the Hall magnetic field in the out-of-plane direction (Birn et al. 2001; Deng & Matsumoto 2001; Ma & Bhattacharjee 2001; Huba & Rudakov 2004; Ren et al. 2005; Lu et al. 2010; Wang et al. 2017; Sang et al. 2018). In symmetric magnetic reconnection, the Hall magnetic field exhibits a quadrupolar structure although the introduction of a guide field will result in the distortion of the quadrupolar structure (Pritchett & Coroniti 2004; Ricci et al. 2004; Huba 2005; Lu et al. 2011; Wang et al. 2012; Huang et al. 2014; Lai et al. 2015; Zhou et al. 2018).

Launched in 2015, the *Magnetospheric Multiscale* (*MMS*) spacecraft has crossed Earth's magnetopause many times, thus providing researchers with opportunities to study asymmetric magnetic reconnection with in situ observations (Burch et al. 2016; Zhou et al. 2016; Wang et al. 2017; Phan et al. 2018). The Hall magnetic field has been revealed by *MMS* observations to have a quadrupolar structure, and both the size and amplitude on the magnetospheric side is much smaller than those on the magnetosheath side (Peng et al. 2017; Wang et al. 2017; Zhang et al. 2017). However, with Cluster measurements, Eriksson et al. (2015) reported an asymmetric reconnection event in the solar wind, and the Hall magnetic field exhibits a hexapolar pattern. Therefore, what kind structure of Hall magnetic field is formed in asymmetric magnetic reconnection is still a puzzle. With a 2D particle-in-cell (PIC) simulation model, we try to investigate the generation of the Hall magnetic field in asymmetric magnetic reconnection. In our companion paper (Paper I), we found that the Hall magnetic field during anti-parallel reconnection in an asymmetric current sheet can evolve from a quadrupolar to a hexapolar structure, and its generation can be explained by the in-plane current system. In this paper, the influence of a guide field on the structure of Hall magnetic field in asymmetric magnetic field is analyzed.

2. Simulation Model

In this paper, a 2D PIC simulation model is employed to investigate the structures of Hall magnetic field during asymmetric magnetic reconnection with a guide field. In the

PIC simulation model, the electromagnetic fields are defined on the grids and renewed by solving the Maxwell equations. The charged particles are advanced by solving the Lorentz equation. Our PIC simulation code has been successfully used to study collisionless magnetic reconnection in the previous works (Fu et al. 2006; Huang et al. 2014; Lu et al. 2016).

The initial configuration of magnetic field, which describes the asymmetric current sheet, is given by

$$\boldsymbol{B}_0(z) = B_0\left[\tanh\frac{z}{\lambda} + R\right]\boldsymbol{e}_x + B_{y0}\boldsymbol{e}_y, \qquad (1)$$

where λ represents the half width of the current sheet, and B_{y0} is the initial guide field. The asymmetry of the magnetic field in the current sheet depends on the parameter R. The ratio of the magnetic field between the side with a stronger magnetic field to that with a weaker magnetic field is $R_B = (1+R)/(1-R)$, where the absolute value of parameter R is less than 1.

The initial number density is given as

$$n(z) = n_0\left(1 - \alpha_1\tanh\frac{z}{\lambda} - \alpha_2\tanh^2\frac{z}{\lambda}\right), \qquad (2)$$

where $\alpha_1 = 2\alpha_2 R$ and $\alpha_2 = B_0^2/[2\mu_0 n_0(T_{e0} + T_{i0}]$, and they are calculated after the pressure balance across the asymmetric current sheet is assumed. The density ratio between the side with a stronger magnetic field to that with a weaker magnetic field is $R_n = (1 - \alpha_1 - \alpha_2)/(1 + \alpha_1 - \alpha_2)$.

The Maxwellian function is assumed for the velocity distribution for both ions and electrons, and their temperatures are uniform in the simulation domain, which are denoted by T_{e0} and T_{i0}, respectively. We set the initial temperature ratio T_{i0}/T_{e0} to be 4. The initial current is contributed by the drift speed of ions and electrons in the direction out of the reconnection plane.

The rectangular simulation domain in the (x, z) plane with the size of $L_x \times L_z = 54d_i \times 22.5d_i$ (where $d_i = c/\omega_{pi}$ is the ion inertial length) are established in this paper, and more than 10^8 for each species of particles are used. The time step is $\Delta t = 0.001\Omega_i^{-1}$, where $\Omega_i = eB_0/m_i$ is the ion cyclotron frequency. The grid size is $\Delta x = \Delta z = 0.05d_i$, thus the grid number in the simulation region is 1080×450. The used light speed is $c/V_A = 15$ (where $V_A = B_0/\sqrt{\mu_0 n_0 m_i}$ is the Alfvén speed), and the mass ratio of ion to electron is $m_i/m_e = 100$. In the z direction, the ideal conducting boundary condition is used for the electromagnetic field, and particles are reflected at the boundary, while the periodic boundary condition is employed for both the electromagnetic field and particles along the x direction. A small flux perturbation is initially added to trigger magnetic reconnection.

3. Simulation Results

A series of runs with different guide field (B_{y0}), ratios of plasma density (R_n) and amplitude of the magnetic field (R_B) between the two sides of the current sheet are performed to study the effect of the guide field on the generation of the Hall magnetic field. Here, the ratio is defined as the value in the upper side of the current sheet over that in the lower side. The parameters of each run are listed in Table 1. In Runs 1–3, the effect of different guide field is analyzed. The effects of the asymmetries of magnetic field and plasma density are investigated in Runs 4–5 and Runs 6–7, respectively.
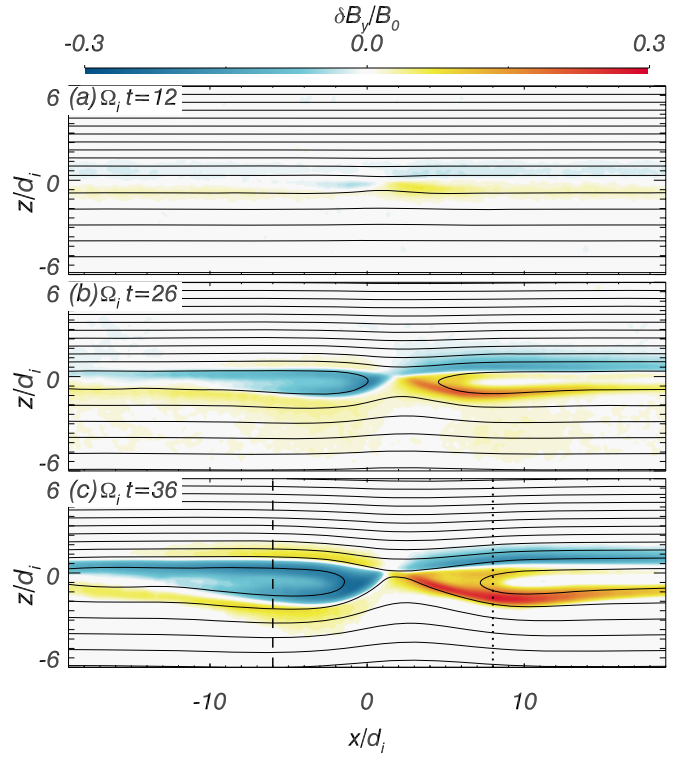

Figure 1. Hall magnetic field $\delta B_y/B_0$ (where $\delta B_y = B_y - B_{y0}$) at $\Omega_i t =$ (a) 12, (b) 26, and (c) 36 for Run 2.

Table 1
The Parameters of Runs 1–7

Run	B_{y0}	R_B	R_n
1	0.2	2	1/3
2	1	2	1/3
3	1.5	2	1/3
4	1	3	1/3
5	1	4	1/3
6	1	2	1/6
7	1	2	1/10

The Hall magnetic field $\delta B_y/B_0$ (where $\delta B_y = B_y - B_{y0}$) at $\Omega_i t =$ (a) 12, (b) 26, and (c) 36 for Run 2 is shown in Figure 1, here $B_0 = B_{y0}$ is the guide field strength. At about $\Omega_i t = 12$, an X line around $(x, z) = (0.0, 0.0)$ begins to be formed, and the reconnection rate increases rapidly. At the same time, the Hall magnetic field begins to be generated in the vicinity of the X line. Then, the Hall magnetic field forms a salient multipolar structure, which is asymmetric between the left and right side of the X line. This can be exhibited clearly at $\Omega_i t = 36$. In the left side of the X line, the Hall magnetic field δB_y has a tripolar structure: in the upper and lower parts the Hall magnetic field δB_y points to the y direction, while it is negative in the central part. On the right side of the X line, the Hall magnetic field δB_y has a bipolar structure. Figure 2 plots the cuts of the Hall magnetic field $\delta B_y/B_0$ along $x = -6d_i$ and $8d_i$ at $\Omega_i t = 36$ for Run 2, which represents the left and right sides of the X line, respectively. The tripolar and bipolar structures on the left and right sides are now shown more clearly. On the left side of the X line, both the amplitude and size of the Hall magnetic field in
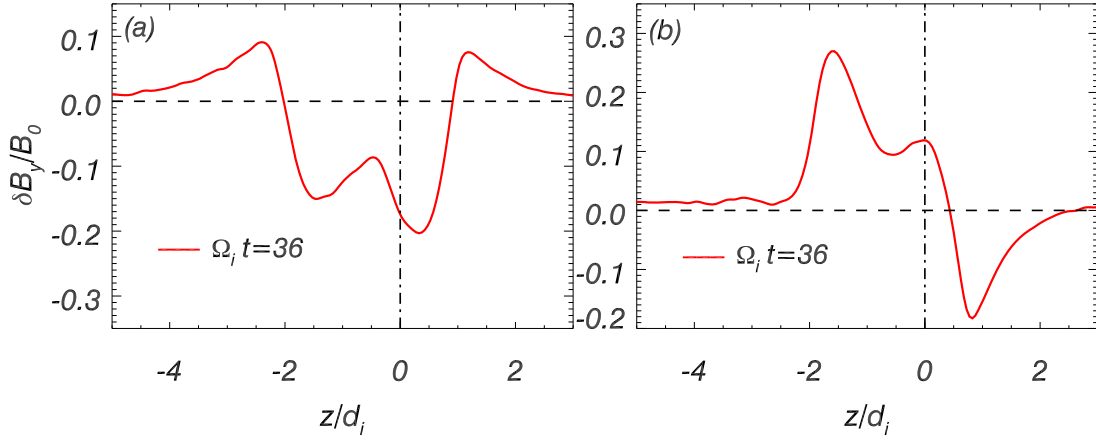
Figure 2. Cuts of the Hall magnetic field $\delta B_y/B_0$ along (a) $x = -6d_i$ (dashed line in Figure 1) and (b) $x = 8d_i$ (dotted line in Figure 1) at $\Omega_i t = 36$ for Run 2.
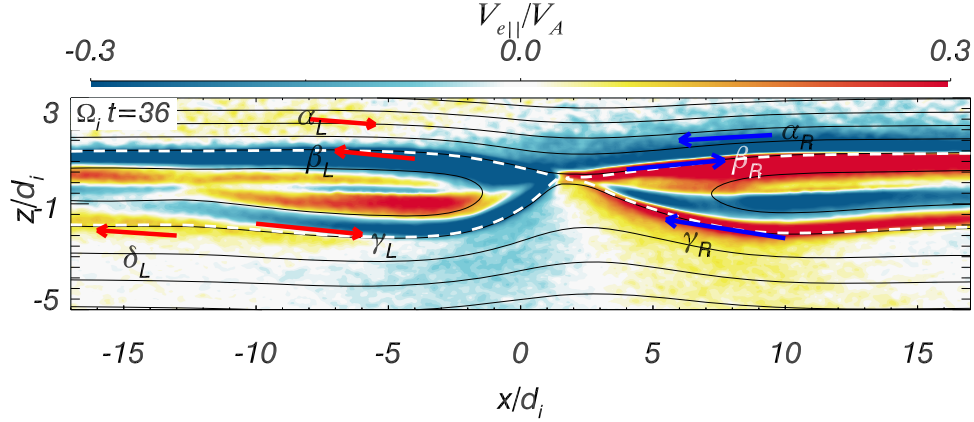

Figure 3. Electron bulk velocity parallel to the in-plane magnetic field ($V_{e\parallel}/V_A$) at $\Omega_i t = 36$ for Run 2.

the central part are much larger than those in the lower and upper parts. On the right side of the X line, the Hall magnetic field in the center part has larger size and amplitude.

Figure 3 plots the electron bulk velocity parallel to the in-plane magnetic field ($V_{e\parallel}/V_A$) at $\Omega_i t = 36$ for Run 2. On both the left and right sides of the X line, the electrons move toward the X line along the separatrices in the lower part of the current sheet, and then leave away from the X line along the separatrices in the upper part of the current sheet. They are denoted by β_L and γ_L on the left side, and by β_R and γ_R on the right side. Above the electron flows β_L and β_R, there still exist two electron flows toward the X line along the magnetic field, which are denoted α_L and α_R on the left and right sides of the X line, respectively. However, on the left side of the X line, we can observe another electron flow below the electron flow γ_L, which moves away from the X line along the magnetic field and is denoted by δ_L. The in-plane current system which is formed by such kind of electron flow leads to the generation of the multipolar structure of the Hall magnetic field described in Figure 1.

In the follows, we will analyze how the guide field (B_{y0}), and ratio of plasma density (R_n) and amplitude of the magnetic field (R_B) between the two sides of the current sheet will influence the multipolar structures of the Hall magnetic field in asymmetric magnetic reconnection.

3.1. The Effect of the Guide Field B_{y0}

The effect of the guide field on the generated Hall magnetic field in asymmetric reconnection is investigated by performing

Runs 1–3. Figure 4 presents the Hall magnetic field $\delta B_y/B_0$ for (a) Run 1 at $\Omega_i t = 35$, (b) Run 2 at $\Omega_i t = 36$, and (c) Run 3 at $\Omega_i t = 39$. At these times, the same magnetic flux ($0.9 V_A B_0$) is reconnected for all three runs. The Hall magnetic field has the same multipolar structure: a tripolar structure on the left side of the X line, and a bipolar one on the right side.

Figure 5(a) shows the corresponding cuts of the Hall magnetic field $\delta B_y/B_0$ along the z direction on the left side of the X line, which are $8d_i$ away from the X line for Runs 1–3 and denoted by the dashed lines in Figure 4. Figure 5(b) describes the ratio of the peak amplitude between Regions A and B, and Regions C and B for Runs 1–3, respectively. Both Regions A and C have positive δB_y, and they are located in the upper and lower parts of the current sheet, respectively. Region B has a negative δB_y and cross the center of the current sheet. With the increasing guide field, the amplitude of the Hall magnetic field in Regions A and B decreases, while that in Region C does not have an obvious trend. However, the ratio of the peak amplitude between Regions C and B increases, while the ratio of the peak amplitude between Regions A and B almost remains as a constant.

Figure 6(a) plots the corresponding cuts of the Hall magnetic field $\delta B_y/B_0$ along the z direction on the right side of the X line, which are $8d_i$ away from the X line for Runs 1–3 and denoted by the dotted lines in Figure 4. Figure 6(b) shows the ratio of the peak amplitude between Regions A and B for Runs 1–3. Here, Region A has a negative value of δB_y and is in the upper part of the current sheet, while Region B has a positive value of
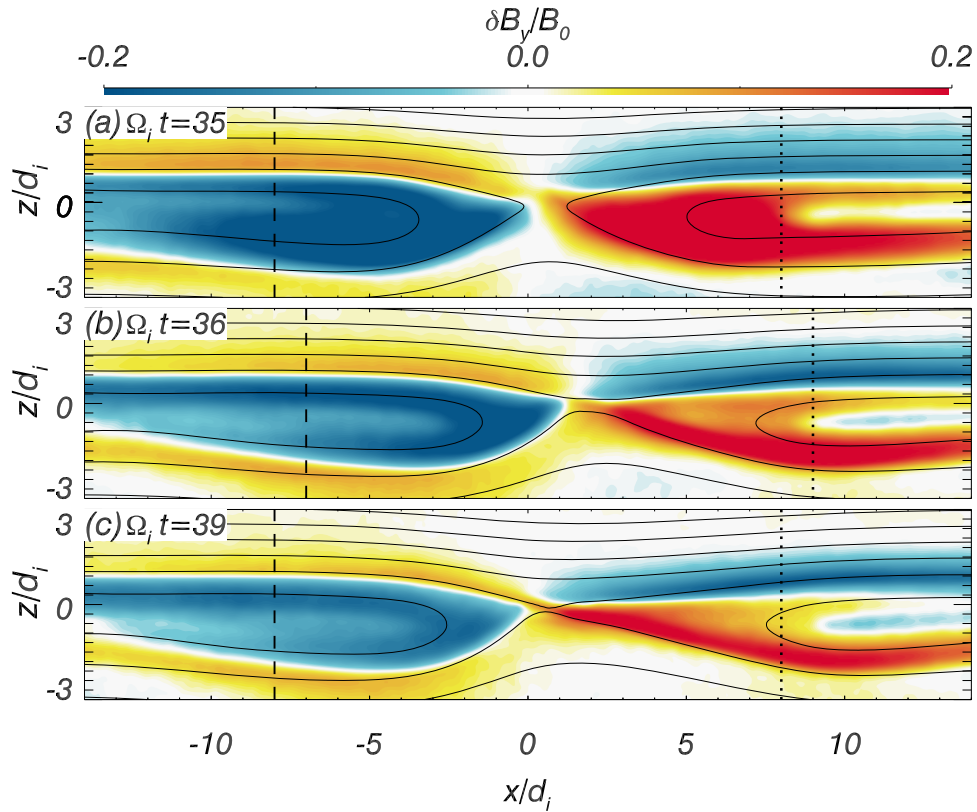
Figure 4. Hall magnetic fields $\delta B_y/B_0$ for (a) Run 1 at $\Omega_i t = 35$, (b) Run 2 at $\Omega_i t = 36$, and (c) Run 3 at $\Omega_i t = 39$.
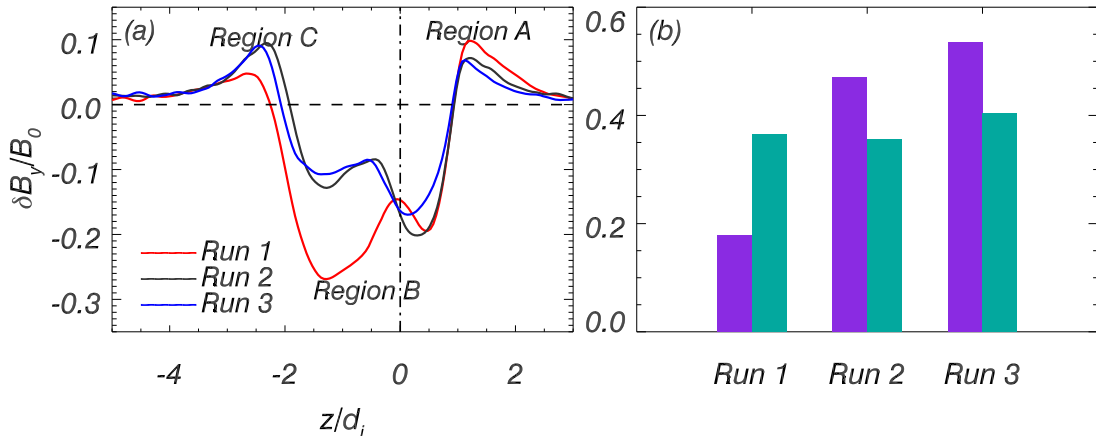

Figure 5. (a) Cuts of the Hall magnetic field $\delta B_y/B_0$ along the z direction on the left side of the X line (dashed lines in Figure 4). (b) Ratios of the peak amplitudes between Regions A and B (cyan bars) and C and B (purple bars).

δB_y and crosses the center of the current sheet. With the increasing guide field, the amplitude of the Hall magnetic field in Region A increases while that in Region B decreases, therefore, the ratio of the peak amplitude between Regions A and B increases.

3.2. The Effect of the Amplitude Ratio of the Magnetic Field R_B

The effect of the amplitude ratio of the magnetic field R_B on the generated Hall magnetic field in asymmetric reconnection is investigated by performing Runs 2, 4–5. Figure 7 presents the Hall magnetic field $\delta B_y/B_0$ for (a) Run 2 at $\Omega_i t = 36$, (b) Run 4 at $\Omega_i t = 47$, and (c) Run 5 at $\Omega_i t = 65$. At these times, the same magnetic flux ($0.9V_A B_0$) is reconnected for all three runs. On the left side of the X line, the structure of the Hall magnetic

field in Runs 4 and 5 is the same as that in Run 2. However, on the right side, the Hall magnetic field Runs 4 and 5 also has a tripolar structure, which is different from that in Run 2.

Figure 8(a) shows the corresponding cuts of the Hall magnetic field $\delta B_y/B_0$ along the z direction on the left side of the X line, which are $8d_i$ away from the X line for Runs 2, 4–5 and denoted by the dashed lines in Figure 7. Figure 8(b) describes the ratio of the peak amplitude between Regions A and B, and Regions C and B for Run 2, 4–5, respectively. Both Regions A and C have positive δB_y, and they are located in the upper and lower parts of the current sheet, respectively. Region B has a negative δB_y and crosses the center of the current sheet. With the increasing amplitude ratio of the magnetic field, the amplitude of the Hall magnetic field in Region A decreases,
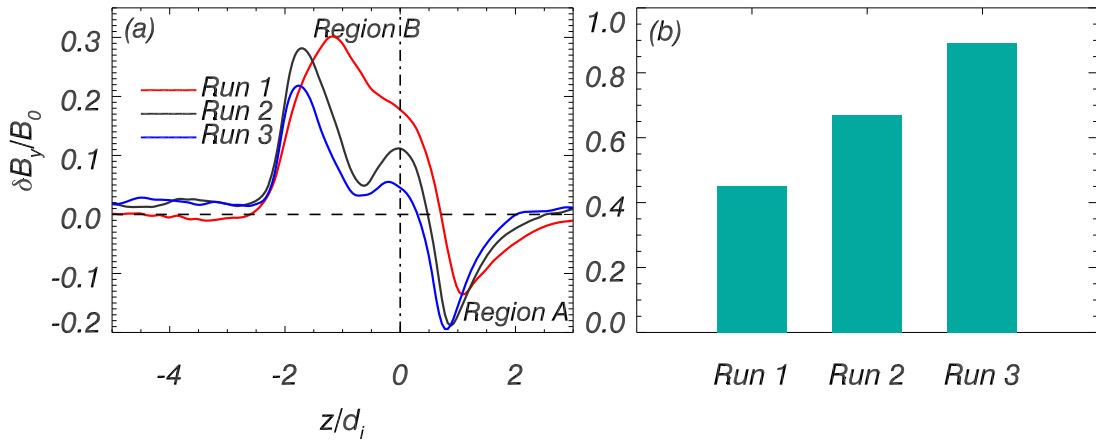
Figure 6. (a) Cuts of the Hall magnetic field $\delta B_y/B_0$ along the z direction in the right side of the X line (dotted lines in Figure 4). (b) Ratios of the peak amplitudes between Regions A and B (cyan bars).
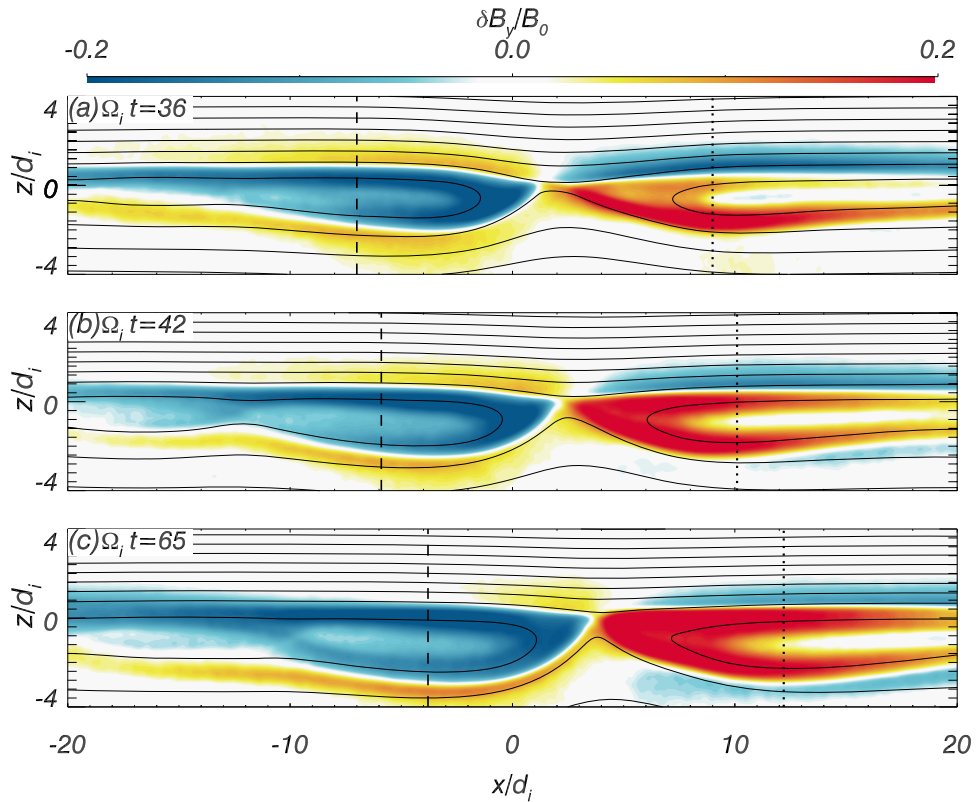

Figure 7. Hall magnetic fields $\delta B_y/B_0$ for (a) Run 2 at $\Omega_i t = 36$, (b) Run 4 at $\Omega_i t = 47$, and (c) Run 5 at $\Omega_i t = 65$.

while that in Regions B and C increase. At the same time, the ratio of the peak amplitude between Regions C and B does not have an obvious tendency, while the ratio of the peak amplitude between Regions A and B decreases.

Figure 9(a) plots the corresponding cuts of the Hall magnetic field $\delta B_y/B_0$ along the z direction on the right side of the X line, which are $8d_i$ away from the X line for Runs 2, 4–5 and denoted by the dotted lines in Figure 7. With the increasing amplitude ratio of the magnetic field, the Hall magnetic field can change from a bipolar structure (Run 2) to a tripolar one (Runs 4–5). Figure 9(b) shows the ratio of the peak amplitudes between Regions A and B for Run 2, and the ratio of the peak amplitude between Regions A and B for Runs 4–5, and Regions C and B for Runs 2, 4–5. Here, Regions A and C have negative δB_y and are in the upper and lower part of the current

sheet, while Region B has a positive value of δB_y and crosses the center of the current sheet. With the increasing guide field, the amplitude of the Hall magnetic field in Region C increases, while that in Region A decreases, and that in Region B does not have an obvious trend. However, the ratio of the peak amplitude between Regions C and B increases and that between Regions A and B decreases.

3.3. The Effect of the Density Ratio R_n

Figure 10 shows the Hall magnetic field $\delta B_y/B_0$ for (a) Run 2 at $\Omega_i t = 36$, (b) Run 6 at $\Omega_i t = 49$, and (c) Run 7 at $\Omega_i t = 63$. At these times, the same magnetic flux $(0.9V_A\ B_0)$ is reconnected for all three runs. On the right side of the X line, the structure of the Hall magnetic field in Runs 6 and 7 is the
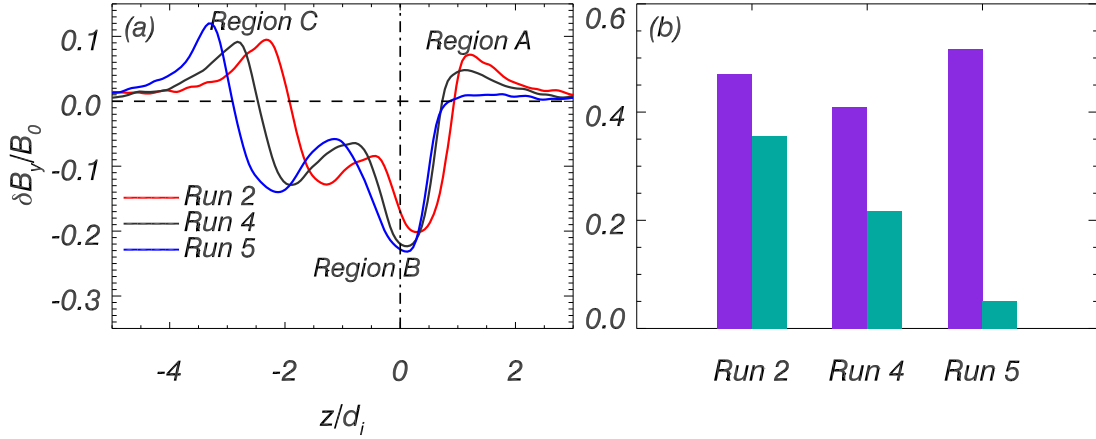
Figure 8. (a) Cuts of the Hall magnetic field $\delta B_y/B_0$ along the z direction in the left side of the X line (dashed lines in Figure 7). (b) Ratios of the peak amplitudes between Regions A and B (cyan bars) and Regions C and B (purple bars).
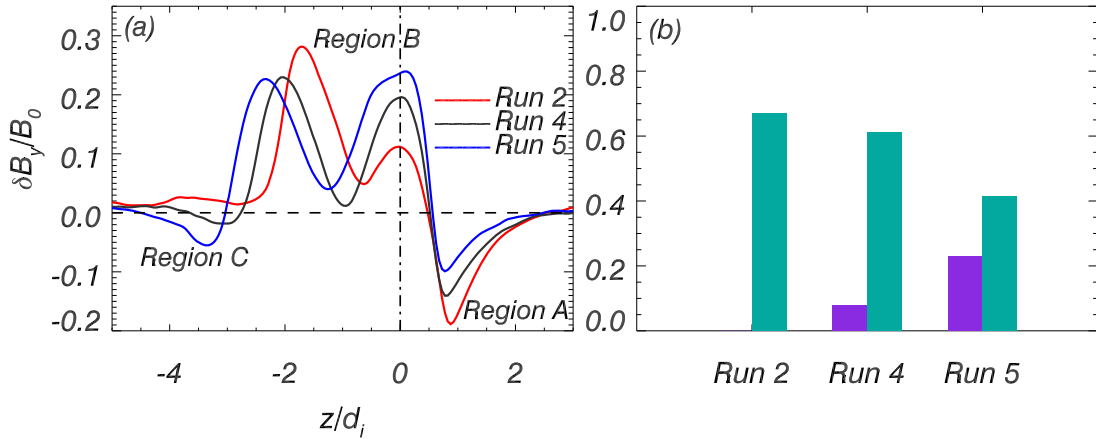

Figure 9. (a) Cuts of the Hall magnetic field $\delta B_y/B_0$ along the z direction in the right side of the X line (dotted lines in Figure 7). (b) Ratios of the peak amplitudes between Regions A and B (cyan bars) and Regions C and B (purple bars).

same as that in Run 2. On the left side, the Hall magnetic field Runs 2 and 6 also has a tripolar structure, and Run 7 has a bipolar structure.

Figure 11(a) shows the corresponding cuts of the Hall magnetic field $\delta B_y/B_0$ along the z direction on the left side of the X line, which are $8d_i$ away from the X line for Runs 2, 6–7 and denoted by the dashed lines in Figure 10. Figure 11(b) describes the ratio of the peak amplitude between Regions C and B for Runs 2, 6–7, respectively. Both Regions A and C have positive δB_y, and they are located in the upper and lower parts of the current sheet, respectively. Region B has a negative δB_y, and crosses the center of the current sheet. With the decreasing density ratio, the amplitude of the Hall magnetic field in Region A decreases until it disappears in Run 7, while that in Region C increases, and that in Region B changes little. Therefore, the ratio of the peak amplitude between Regions C and B increases with the decrease of the density ratio.

Figure 12(a) plots the corresponding cuts of the Hall magnetic field $\delta B_y/B_0$ along the z direction on the right side of the X line, which are $8d_i$ away from the X line for Runs 2, 6–7 and denoted by the dotted lines in Figure 10. Figure 13(b) shows the ratio of the peak amplitude between Regions A and B. Here, Region A has a negative value of δB_y, and is in the upper part of the current sheet, while Region B has a positive value of B_y and crosses the center of the current sheet. With the decreasing density ratio, the amplitude of the Hall magnetic

field in Region A decreases while that in Region B changes little, therefore, the ratio of the peak amplitude between Regions A and B decreases.

4. Conclusions and Discussion

In this paper, we perform 2D PIC simulations to investigate the structure of Hall magnetic field during asymmetric magnetic reconnection with a guide field. The introduction of the guide field will lead to the difference of the Hall magnetic field structure between the left and right side of the X line. The Hall magnetic field on the left side of the X line tends to have a tripolar structure: the Hall magnetic field at the upper and lower parts of the current have positive values, and that at the central part has a negative value. With the increase of the guide field, the Hall magnetic field at the upper and central parts of the current sheet decreases, and that at the lower part increases. While the increasing asymmetry of the current sheet will enhance the Hall magnetic field at the central and lower parts of the current sheet and decrease of the Hall magnetic field at the upper part. When the asymmetry is sufficiently large, the Hall magnetic field at the upper part will even disappear and results in the bipolar structure. The Hall magnetic field on the right side of the X line tends to have a bipolar structure: the Hall magnetic field at the upper part is negative, and that at the central part is positive. With the increase of the guide field, the Hall magnetic field at the upper part of the current sheet will
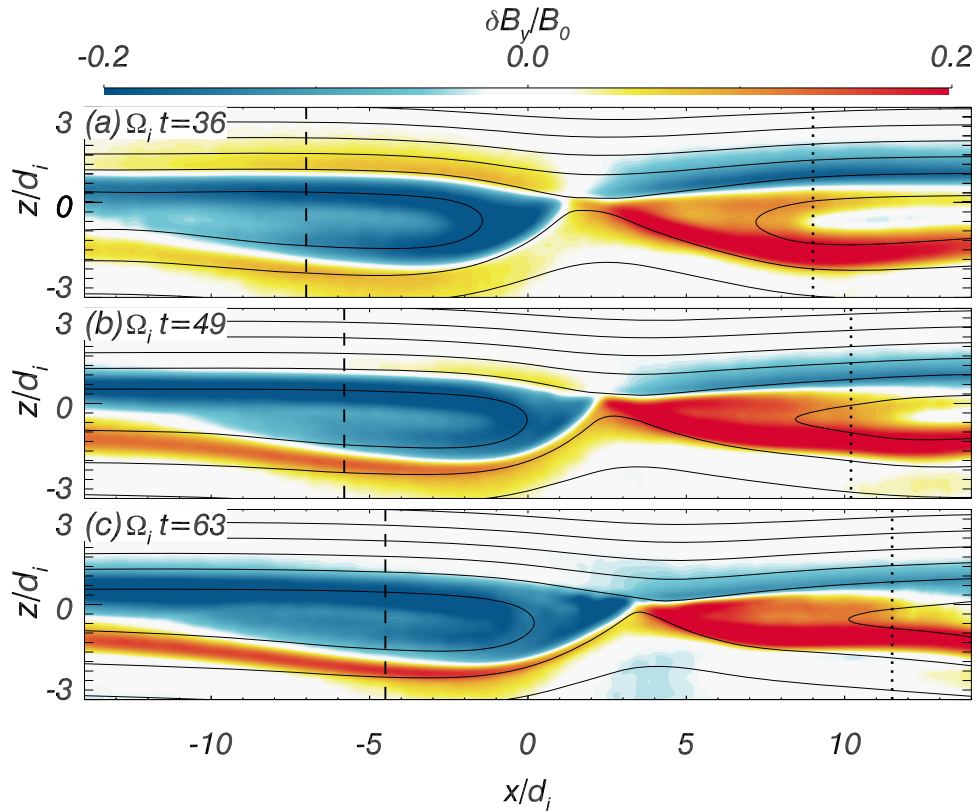
Figure 10. Hall magnetic fields $\delta B_y/B_0$ for (a) Run 2 at $\Omega_i t = 36$, (b) Run 6 at $\Omega_i t = 49$, and (c) Run 7 at $\Omega_i t = 63$.
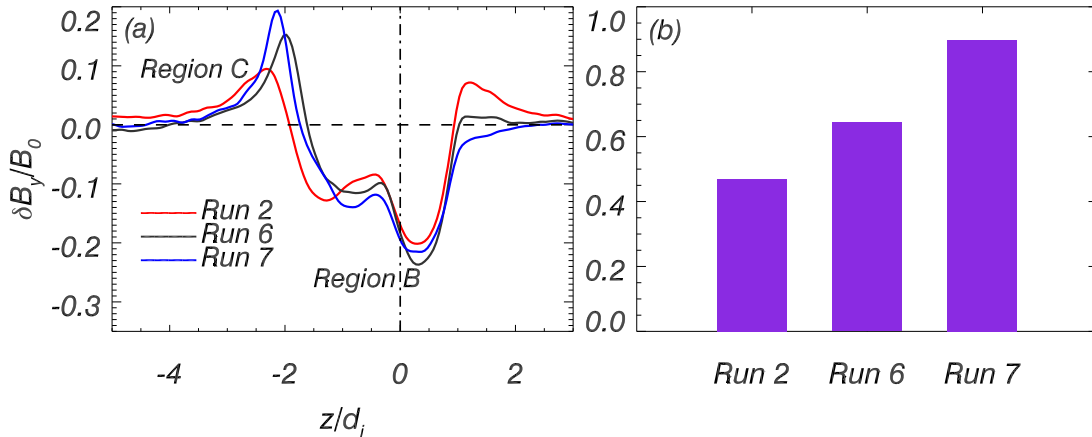

Figure 11. (a) Cuts of the Hall magnetic field $\delta B_y/B_0$ along the z direction in the left side of the X line (dashed lines in Figure 10). (b) Ratio of the peak amplitudes between Regions C and B (purple bars).

also increase, while that at the central part will decrease. The increasing asymmetry of the current sheet will result in a decrease of the Hall magnetic field at the upper and central parts of the current sheet, however, when the asymmetry is sufficiently large, there will appear a Hall magnetic field with a negative value below that at the central part and a tripolar structure of the Hall magnetic field is at last formed.

The characteristics of the Hall magnetic field in asymmetric reconnection heavily depend on the guide field and the asymmetry of the current sheet. The introduction of a guide field will lead to the difference of the Hall magnetic field between the left and right sides of the X line. The difference between the left and right sides of the X line is caused by the diamagnetic drift of the X line in the outflow direction, as

discussed by Swisdak et al. (2003). On the left side of the X line, the increasing asymmetry of the current sheet will result in the change of the Hall magnetic field from a tripolar to bipolar structure on the left side. On the right side of the X line, the increasing ratio of the magnetic field tends to change the Hall magnetic field from a bipolar to a tripolar structure, while the Hall magnetic field seems to remain a bipolar structure with the increasing density ratio.

The *MMS* spacecraft, which was launched in 2015 and has crossed the magnetopause many times, has provided us opportunities to study the characteristics of asymmetric magnetic reconnection. Both bipolar and tripolar structure of the Hall magnetic field have been observed in magnetopause reconnection (Eriksson et al. 2016; Peng et al. 2017; Wang et al. 2017;
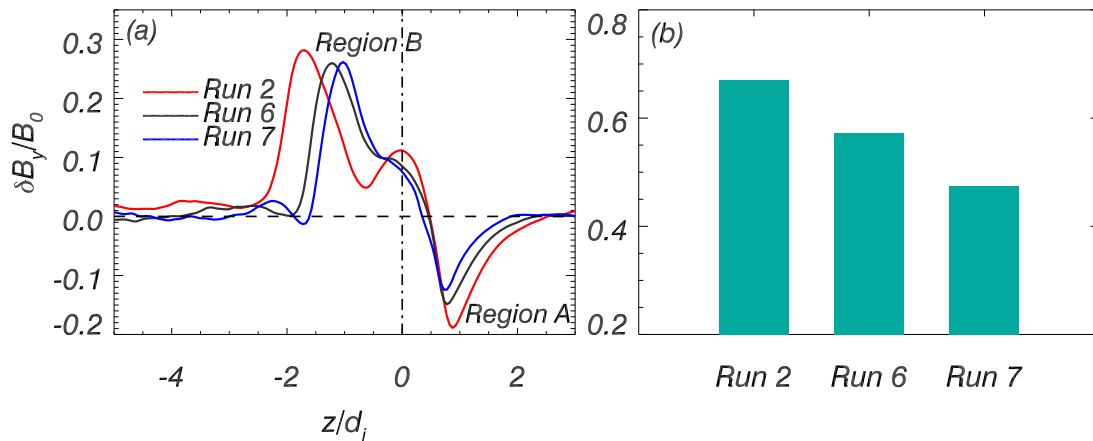
Figure 12. (a) Cuts of the Hall magnetic field $\delta B_y/B_0$ along the z direction in the right side of the X line (dotted lines in Figure 10). (b) Ratio of the peak amplitudes between Regions A and B (cyan bars).

Zhang et al. 2017; Sturner et al. 2018), however, more observations are necessary to confirm our prediction on the dependence of the Hall magnetic field on the asymmetry of the current sheet, which is our future plan.

ORCID iDs

Quanming Lu ⓘ https://orcid.org/0000-0003-3041-2682

References

Angelopoulos, V., McFadden, J. P., Larson, D., et al. 2008, Sci, 321, 931
Birn, J., Drake, J. F., Shay, M. A., et al. 2001, JGR, 106, 3715
Birn, J., Fletcher, L., Hesse, M., & Neukirch, T. 2009, ApJ, 695, 1151
Biskamp, D., & Schwarz, E. 1995, PhRvL, 75, 3850
Burch, J. L., Torbert, R. B., Phan, T. D., et al. 2016, Sci, 352, aaf2939
Deng, X. H., & Matsumoto, H. 2001, Natur, 410, 557
Drake, J. F., Swisdak, M., Che, H., & Shay, M. A. 2006, Natur, 443, 553
Eriksson, S., Cassak, P. A., Retinó, A., & Mozer, F. S. 2016, GeoRL, 43, 3035
Eriksson, S., Lapenta, G., Newman, D. L., et al. 2015, ApJ, 805, 43
Forbes, T. G., & Acton, L. W. 1996, ApJ, 459, 330
Fu, X. R., Lu, Q. M., & Wang, S. 2006, PhPl, 13, 012309
Gosling, J. T., & Birn, J. 1995, GeoRL, 22, 869
Huang, C., Lu, Q., Guo, F., et al. 2015, GeoRL, 42, 7282
Huang, C., Lu, Q., Lu, S., Wang, P. R., & Wang, S. 2014, JGRA, 119, 798
Huba, J. D. 2005, PhPl, 12, 012322
Huba, J. D., & Rudakov, L. I. 2004, PhRvL, 93, 175003
Isobe, H., Takasaki, H., & Shibata, K. 2005, ApJ, 632, 1184

Lai, X. S., Zhou, M., Deng, X. H., et al. 2015, ChPhL, 32, 095202
Lin, J., & Forbes, T. G. 2000, JGR, 105, 2375
Lu, Q. M., Huang, C., Xie, J. L., et al. 2010, JGRA, 115, A11208
Lu, S., Lin, Y., Angelopoulos, V., et al. 2016, JGRA, 121, 11882
Lu, S., Lu, Q. M., Huang, C., et al. 2011, ChSBu, 56, 48
Lu, S., Lu, Q. M., Huang, C., & Wang, S. 2013, PhPl, 20, 061203
Ma, Z. W., & Bhattacharjee, A. 2001, JGR, 106, 3773
Øieroset, M., Phan, T. D., Fujimoto, M., et al. 2001, Natur, 412, 414
Parker, E. N. 1957, JGR, 62, 509
Peng, F. Z., Fu, H. S., Cao, J. B., et al. 2017, JGRA, 122, 6349
Phan, T. D., Eastwood, J. P., Shay, M. A., et al. 2018, Natur, 557, 202
Pritchett, P. L., & Coroniti, F. V. 2004, JGRA, 109, A01220
Qiu, J., Wang, H. M., Cheng, C. Z., & Gary, D. E. 2004, ApJ, 604, 900
Ren, Y., Yamada, M., Gerhardt, S., et al. 2005, PhRvL, 95, 055003
Ricci, P., Brackbill, J. U., Daughton, W., & Lapenta, G. 2004, PhPl, 11, 4102
Roald, C. B., Sturrock, P. A., & Wolfson, R. 2000, ApJ, 538, 960
Sang, L. L., Lu, Q. M., Wang, R. S., et al. 2018, PhPl, 25, 062120
Somov, B., & Kosugi, T. 1997, ApJ, 485, 859
Sonnerup, B. U. Ö. 1971, JGR, 76, 6717
Sturner, A. P., Eriksson, S., Nakamura, T., Gershman, D. J., et al. 2018, JGRA, 123, 1305
Sweet, P. A. 1958, in IAU Symp. 6, Electro-magnetic Phenomena in Cosmical Physics, ed. B. Lehnert (Cambridge: Cambridge Univ. Press), 123
Swisdak, M., Rogers, B. N., Drake, J. F., & Shay, M. A. 2003, JGRA, 108, 1218
Tsuneta, S. 1996, ApJ, 456, 840
Wang, R. S., Lu, Q. M., Nakamura, R., Huang, C., et al. 2016, NatPh, 12, 263
Wang, R. S., Nakamura, R., Lu, Q. M., et al. 2012, JGRA, 117, A07223
Wang, R. S., Nakamura, R., Lu, Q. M., et al. 2017, PhRvL, 118, 175101
Yamada, M., Yoo, J., Jara-Almonte, J., et al. 2014, NatCo, 5, 4774
Zhang, Y. C., Lavraud, B., Dai, L., et al. 2017, JGRA, 122, 5277
Zhou, M., Ashour-Abdalla, M., Berchem, J., et al. 2016, GeoRL, 43, 4808
Zhou, M., Berchem, J., Walker, R. J., et al. 2018, JGRA, 123, 1834
Zhou, M., Berchem, J., Walker, R. J., & El-Alaoui, M. 2017, PhRvL, 119, 055101